Engineered Science
DOI: https://dx.doi.org/10.30919/es1372

Drag and Heat Reduction for Blunt Bodies in Hypersonic Flows Using a Novel Double Aerodisk

Mohamed A. Mohamed,[1, 2] Buse Nur Bekir,[1] Kürşad Melih Güleren,[3] Muhammad Faizan[4] and Imran Afgan[4, 5,*]

Abstract

High speed aerodynamic drag and heating are the two major causes of concern in fly missions of hypersonic vehicles. For such flows, installing an aerospike in front of the vehicle's nose has been an effective solution for reducing wave drag and thermal loads over the vehicle's body for years. In this study, a novel design of the blunt nose attached with a double-aerospike for hypersonic vehicles is proposed, which reduces both the drag and the aerodynamic heating. The fluid and thermal fields around the double-aerospike at the ratio of spike length (L) to diameter of the blunt body (D) of 2 and various angles-of-attack (AOA) are investigated numerically using ANSYS-Fluent at a Mach number of 6. The results show a good agreement with the available experimental data of a flat-faced attached single aerospike and that the novel double aerospike significantly reduces the drag coefficient by 15.55% and 29.23% at 5° and 8° angles-of-attack, respectively, compared to the single spiked configuration. The novel double aerospike reduces the aerodynamic heating for all the studied angles-of-attack (α=0°, 5° & 8°). The modified configuration also shows a reduction in the temperature difference between the upper and lower frontal areas of the blunt body by 96.25% at 8° AOA compared to the single spike model.

Keywords: Aerodynamic heating; Double aerospike; Hypersonic flow; Wave drag.
Received: 18 January 2024; Revised: 21 July 2024; Accepted: 02 October 2024.
Article type: Research article.

1. Introduction

Over a decade after the retirement of the Concorde supersonic aircraft, industrial companies and researchers are not only looking to bring back supersonic aircraft but also hoping to make hypersonic passenger aircraft a reality.[1] However, in hypersonic vehicles, the vehicle nose is subjected to serious aerodynamic heating and strong shock wave drag problems, which can burn it out and narrow the flight range. The deteriorated effect of these two problems resulted from their excessive negative contribution to the vehicle drag and thermal loads, hence poor aerodynamic performance. Therefore, reducing the negative effects of both phenomena is the most challenging design requirement for aerospace vehicles.

Although flow separation is an avoidable situation in general aerodynamic applications because it causes energy loss, it can be desirable under particular conditions, such as a blunt body traveling at supersonic or hypersonic speed.[2] Although the blunt nose shape was approved to reduce the aerodynamic heating, however, it increases the aerodynamic drag of the hypersonic vehicle. Hence, several techniques have been proposed to reduce the aerodynamic drag of hypersonic vehicles, such as energy deposition, aerospike, opposing jet, and a combination of aerospike and opposing jet.[3-6] Among all these techniques, aerospike showed a remarkable reduction in both aerodynamic heating and wave drag. Attaching an aerospike to the nose of a blunt body causes a flow separation, which develops into a conical shock wave. [7] The shock wave structure from normal to oblique shock wave - which provokes the drag reduction considerably.[8,9] This type of separation creates a shield for the blunt body from incoming flow, hence leading the vehicle to drag and heat reduction and lift increase.[10]

[1] *Aerospace & Mechanical Engineering, University of South Wales, Pontypridd, CF37 1DL, United Kingdom*
[2] *Department of Mechanical Engineering, Faculty of Engineering, South Valley University, Qena, 83523, Egypt*
[3] *Eskisehir Osmangazi University, Faculty of Engineering and Architecture, Department of Aeronautical Engineering, 26040, Turkey*
[4] *Department of Mechanical and Nuclear Engineering, College of Engineering, Khalifa University, Abu Dhabi, 127788, UAE*
[5] *Department of Mechanical and Aerospace Engineering, The University of Manchester, Sackville Street, Manchester, M13 9PL, United Kingdom*
**Email:* imran.afgan@ku.ac.ae (I. Afgan)

In 1947, Alexander introduced the positive effect of attaching an aerospike to reduce drag on blunt bodies at supersonic speeds.[11] A few years later, in 1952, a wind tunnel test was carried out by Beastall and Turner to investigate different spike combinations, such as using cone-attached spikes with semi-angles of 15°, 30° and 40°.[12] The results were compared against the results of using a blunt body without a cone-attached spike at Mach numbers of 1.5, 1.6 and 1.8, which showed that the blunt body with a 15° semi-angle conical nose-attached spike achieved the minimum drag coefficients of 0.47, 0.27 and 0.21 at Mach numbers of 1.5, 1.6 and 1.8, respectively. In the same year, Jonesconducted an experimental study to investigate the effect of cone angle and spike length on the drag coefficient of high-speed vehicles.[13] The results obtained from his study showed that the short-rod spike model was causing higher pressure in the separated region than on the cone surface, and the blunt body with 20∘ semi-angle cone attached spike achieved the minimum drag coefficient (CD=0.156) compared to the conventional nose (C_D=0.550). Furthermore, a dead air region was created near the reattachment point by shock waves linked to spike length. Another study was conducted by Mair in 1952,[14] which showed that if the blunt body has a hemispherical nose shape instead of a flat one, the dead air region is perceptibly moved away from the blunt body's shoulder. As a result, the reattachment shock is carried further away from the shoulder of the blunt body, especially when the boundary layer on the spike is laminar. Because the researchers at that time were keen to understand the behavior of the flow under different geometrical nose combinations, they focused only on cone windshield-attached spikes, such as Jones's work.[13]

In 1960, the hypersonic flow behavior over different types of spiked bodies was studied experimentally using the hypersonic gun tunnel of Imperial College at Mach number 6.8.[15] According to Schlieren's photographs taken from those experiments, attaching the spike to a blunt body with a flat-faced nose was insufficient for a steady flow. However, the flow was predictable and steady if the nose had a hemispherical shape. Alongside the drag coefficient and obtaining the flow behavior, heat distribution over a spiked blunt body was another issue that needed more investigation. Experimental studies have been conducted at Mach numbers 10 and 15 in a gun tunnel to investigate the total heat distribution and reattachment over geometrically similar but slightly different spike-attached blunt body configurations.[16] The results showed that the L/D ratio greater than 3 was the optimum configuration for decreasing the total heat transfer. Another vital observation was that on the spiked hemispherical body, the total heat transfer rates were reduced to less than one-fifth with basic coned body geometry with attached spike, and there was no issue, such as local heat increases in the reattachment region. As much as heat distribution in the hypersonic flow field at different regions, the pressure distribution is also an important parameter to consider. Therefore, experimental studies were performed to observe fluctuating pressure over a disk-tipped spike-attached blunt body by Guenther and Reding in 1977.[17] According to experimental results, the distributions of both overall fluctuating and static pressure coefficients were consonant well. However, static pressure increased with a Mach number of up to 1.2 and decreased to a constant value at a Mach number of 2.5 and higher. The last quarter of the 20th century conveyed a host of computational innovations, and mathematical solutions were integrated into computers. Therefore, understanding the flow behavior was one of these curiosities that scientists were keen to discover.

In 1981, Myshenkov numerically studied the flow separation over a spiked blunt body in the range of Mach numbers from 1.75 to 14.[18] The solution of Navier-Stokes equations showed that the pressure on the spike was most commonly a constant at the separation region and was equal to the pressure in the oncoming flow at a large Reynolds number. A few years later, Shoemaker studied missile systems with hemispherical nose blunt bodies attached with biconical tip spikes for a range of Mach numbers (1.5 to 3) and spike lengths (2 to 9 inches).[19] According to computational results, an increase in the spike length causes a decrease in the axial force coefficient until the length reaches 5 inches, afterward, increasing the spike length causes the drag to increase. In 1995, another detailed numerical study was coded and performed to investigate the hypersonic flow behavior around the spiked blunt body with $0^{\circ}$and 10°angles-of-attack.[20] The effects of spike's length, angles-of-attack and Mach number were examined. The best result obtained was at $L/D = 2$, which gave a drag coefficient of $C_D = 0.32$. In 2002, Mehta studied numerically the pressure oscillations over a spiked axisymmetric blunt body at Mach number of 6.80 and for spike length to hemispherical diameter ratios of 0.5, 1.0 and 2.0.[21] The maximum pressure distribution of the spiked blunt body was found to be at 40° for all L/D ratio variations. However, the peak point of pressure on the blunt-body decreased with extending the spike length. A few years later, Mehta, Kalimuthu and Rathakrishnan carried out an experimental study on spiked models with different nose tips, range of AOA at 0°, 5° and 8°, Mach number of 6 and L/D = 1.5 and 2.[22] The spike models had different nose geometries, such as conical aerospike, hemisphere aerodisk and flat-faced aerodisk. According to experimental results, the spike with aerodisk with the L/D ratio equal to 2 is the most effective model from the drag reduction point of view. The researchers in the literature review investigated the hypersonic flow and the related drag and heat characteristics for spiked bunt bodies and the effect of some parameters such as spike length, angle of attack and spike nose geometry. Recently, different aerospikes combinations for discovering its beneficial phenomenon's limitations have been carried out. For example, lengthening the aerospike does not cause drag reduction if the length exceeds four times the blunt body diameter.[5,23-26] Further studies were carried out experimentally and numerically to understand the physics of high-speed flows

past blunt bodies attached with spikes having different nose geometries.[27,28] Because drag and aerodynamic heating are significant challenges for hypersonic vehicles such as space shuttles, therefore investigating novel solutions to reduce drag and heat over a blunt body can be considered more important now to have an advantage for further space exploration.

In the present study, a novel idea of using a double-spike design attached to a blunt body is investigated numerically using the computational fluid dynamics (CFD) approach in ANSYS-Fluent software for hypersonic drag and aerodynamic heating reduction. The new configuration is studied at Mach number of 6, three angles of attack of 0°, 5° and 8°, L/D ratio of 2 and spike nose geometry of flat-faced aerodisk. As this novel mechanism has never been conducted before, hence analyzing the results will be crucial for future investigations.

2. Numerical approach

2.1 Flow governing equations

When the flow over the bunt bodies becomes supersonic or hypersonic, a shock wave forms and interacts with the boundary layer. The attached spike causes a flow separation in front of the blunt body, hence, drag and aerodynamic heating are reduced significantly. The generated flow field in such a phenomenon is quite complicated and includes different flow regions, as seen in Fig. 1. Separation region occurs after the flow meets the tip of the aerospike; hence, shock waves are generated. Furthermore, the expended flow starts where the hypersonic flow meets the aero disc. The flow field around a spike attached body at supersonic and hypersonic speeds contains different flow types, and different phenomena, which need to be studied. Therefore, the ANSYS software package is used in the current study with a fully unstructured finite volume solver. The suitability of the solver has been extensively benchmarked in the past by the authors, see Refs. [29-33].

The CFD model used is based on solving the system of two-dimensional Navier-Stokes equations of steady, viscous and turbulent flow over the hemispherical body nose.[34,35]

$$\text{Continuity:} \quad \frac{\partial}{\partial x}(\rho u) + \frac{\partial}{\partial y}(\rho v) = 0 \tag{1}$$

$$\text{x- Momentum:} \quad \frac{\partial}{\partial x}(\rho u^2 + p - \tau_{xx}) + \frac{\partial}{\partial y}(\rho uv - \tau_{yx}) = 0 \tag{2}$$

$$\text{y- Momentum:} \quad \frac{\partial}{\partial x}(\rho uv - \tau_{xy}) + \frac{\partial}{\partial y}(\rho v^2 + p - \tau_{yy}) = 0 \tag{3}$$

$$\text{Energy:} \quad \frac{\partial}{\partial x}\left[(E_t + \rho)u + q_x - u\tau_{xx} - v\tau_{xy}\right] + \frac{\partial}{\partial y}\left[(E_t + \rho)v + q_y - u\tau_{yx} - v\tau_{yy}\right] = 0 \tag{4}$$

In the simulation, a perfect gas assumption of incoming flow is made, viscosity is calculated as $\mu = 2.498 \times 10^{-5} kg/m.s$ using Sutherland's law. The calculations have been carried out with interpolation for $450°K$,[36] as indicated in Table 1. The expected heat transfer to the wall, $\dot{q}_w$, can be determined using Fourier law as $\dot{q}_w = \left(\frac{\partial T}{\partial n}\right)_w$ at the wall.

Table 1: Incoming flow parameters at $450°K$.

Temperature, K	Density, $\rho, kg/m^3$	Dynamic viscosity, $\mu, kg/m.s$	Kinematic viscosity, $v, m^2/s$	Prandtl Number, P_T
433.15	0.8148	2.420×10^{-5}	2.975×10^{-5}	0.7014
450	0.7811	2.491×10^{-5}	3.175×10^{-5}	0.7010
453.15	0.7788	2.504×10^{-5}	3.212×10^{-5}	0.6992

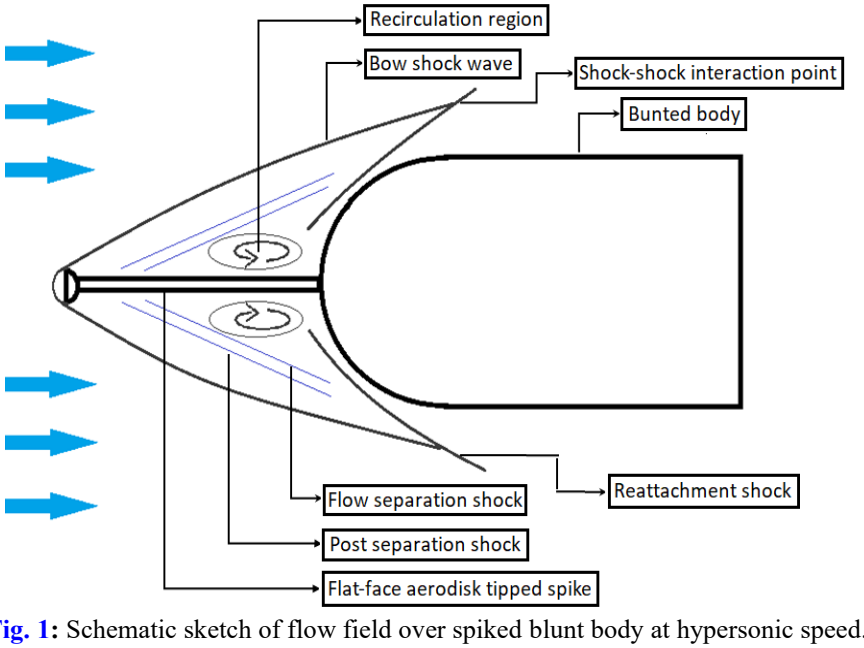

Fig. 1: Schematic sketch of flow field over spiked blunt body at hypersonic speed.

2.2 Turbulence model

The recirculation regions and possible other vortex regions in the flow field of the novel double-spike are predicted by solving the compressible flow with heat transfer using the $k-\omega\ SST$ turbulence model. The equations of the standard Wilcox SST two-dimensional equation model for time-independent flow are outlined below.[37]

$$\frac{\partial(\rho u_j k)}{\partial x_j} = P - \beta^*\rho\omega k + \frac{\partial}{\partial x_j}\left[\left(\mu + \sigma_k\frac{\rho k}{\omega}\right)\frac{\partial k}{\partial x_j}\right] \quad (5)$$

$$\frac{\partial(\rho u_j \omega)}{\partial x_j} = \frac{\gamma\omega}{k}P - \beta\rho\omega^2 + \frac{\partial}{\partial x_j}\left[\left(\mu + \sigma_\omega\frac{\rho k}{\omega}\right)\frac{\partial\omega}{\partial x_j}\right] + \frac{\rho\sigma_d}{\omega}\frac{\partial k}{\partial x_j}\frac{\partial\omega}{\partial x_j} \quad (6)$$

where:

$$P = \tau_{ij}\frac{\partial u_i}{\partial x_j},\ \tau_{ij} = \mu_t\left(2S_{ij} - \frac{2}{3}\frac{\partial u_k}{\partial x_i}\delta_{ij}\right) - \frac{2}{3}\rho k\delta_{ij},\ S_{ij} = \frac{1}{2}\left(\frac{\partial u_i}{\partial x_j} + \frac{\partial u_i}{\partial x_j}\right),\ \mu_t = \frac{\rho k}{\hat{\omega}} \quad (7)$$

The turbulence model is implemented into compressible, time-independent Reynolds-averaged navier-stokes (RANS) equations, as follows.[38]

$$\frac{\partial}{\partial x_j}\left(\overline{\rho u_j}\right) = 0 \quad (8)$$

$$\frac{\partial}{\partial x_j}\left(\overline{u_j\rho u_i}\right) = -\frac{\partial p}{\partial x_i} + \frac{\partial\overline{\sigma_{ij}}}{\partial x_j} + \frac{\partial\tau_{ij}}{\partial x_j} \quad (9)$$

$$\frac{\partial}{\partial x_j}\left(\hat{u}_j\overline{\rho}\hat{H}\right) = \frac{\partial}{\partial x_j}\left(\overline{\sigma_{ij}\hat{u}_i} + \overline{\sigma_{ij}\hat{u}_i''}\right) - \frac{\partial}{\partial x_j}\left(\overline{q_j} + c_p\overline{\rho u_j''T''} - \hat{u}_j\tau_{ij} + \frac{1}{2}\overline{\rho u_i''u_i''u_j''}\right) \quad (10)$$

2.3 Y^+ calculations

In this study, the turbulent Reynolds number is calculated at Mach number of 6 and $T_\infty = 450K$ as $Re_l = \rho UL/\mu \simeq 5\times10^6$. A mesh with high quality was created to solve this flow field accurately. No-slip boundary conditions were applied to the spike attached to the blunt body's surface. Moreover, the flow immediately next to the wall is essentially laminar because the effects of turbulence are relatively small. This situation is called a viscous sublayer for RANS simulations. The normal velocity component v_n with respect to n must be zero at the stationary wall. Hence, the normal viscous stress, τ_{nn}, which is equal to zero, and the parallel velocity component, v_t, gives the shear stress, τ_{nt}, as shown in the equation below.[39]

$$\tau_{nn} = 2\mu\left(\frac{\partial v_n}{\partial n}\right)_{wall} = 0 \quad (11)$$

$$\tau_{nt} = \mu\left(\frac{\partial v_t}{\partial n}\right)_{wall} \quad (12)$$

In this study, hypersonic flow is investigated over a spike-attached blunt body. Thus, the distance of the first cell layer from the no-slip wall surface is calculated as extremely thin, and the aspect ratio becomes ultimately high. Therefore, the generalized scaling law was obtained, and the friction velocity equation was developed based on $\tau_{wall} = |\tau_{nt}|$.[40]

$$u_\tau = \sqrt{\frac{\tau_{wall}}{\rho}} \quad (13)$$

$$\tau_{wall} = \frac{1}{2}C_f\rho u_\infty^2 \quad (14)$$

Once wall boundary conditions are implemented in RANS Navier-Stokes turbulent flow model, the first cell layer distance, $\triangle y_p$ is calculated from below equation.

$$Y^+ = \frac{\triangle y_p}{v}u_\tau \quad (15)$$

The Y^+ value should be between 1.0 to 5.0 to have a pure viscous sublayer, which is also the wall treatment used in the current $k-\omega\ SST$ turbulence model simulations. As a further matter, C_f is the skin friction coefficient on a plate and it was generalised for $5\times10^5 < Re_x < 10^7$ as $C_f = 0.0592Re_x^{-1/5}$. Therefore, the first cell layer distance is calculated as $\triangle y_p = 0.00045mm$ for $Y^+ = 0.1$.

2.4 Aerodynamic heat and drag calculations

Aerodynamic heating arises as the main problem during the design of hypersonic vehicles due to the high speed. The calculation process of aerodynamic heating can be accomplished in three stages. The first stage is to solve the hypersonic inviscid flow field using modified Newton theory to obtain the flow parameters in the region outer the boundary layer.[41] Second, solving the viscous boundary layer region to obtain the aerodynamic heating coefficient on the body surface using reference enthalpy method and Reynolds analogy. Finally, solving the Fourier conductive heat transfer equation to determine the surface temperature distribution.[42] The flow parameters in the area outside the boundary layer are assumed to equal to that the free stream conditions ahead the blunt body, namely,

$$v = v_\infty, P = P_\infty, T = T_\infty, Ma = Ma_\infty \quad (16)$$

where v_∞ is the inlet flow speed, P_∞ is the inlet flow pressure, T_∞ is the inlet flow temperature, and Ma_∞ is the inlet mach number.

For hypersonic flows ($Ma_\infty > 5$), which is the current case, a detached shock wave appears ahead of the aerospike which can be calculated using the normal shock relationships.[43] According to Prandtl- Meyer expansion wave phenomena, the leading edge of the expansion fan is continuous with an angle of μ_1 concerning the upstream flow direction, and with respect to the downstream flow direction, wave's trailing edge makes an angle of μ_2. The relationship between the angles and the Mach number is defined as $\mu_1 = sin^{-1}(1/M_1)$ and $\mu_2 = sin^{-1}(1/M_2)$, as shown in Fig. 2.

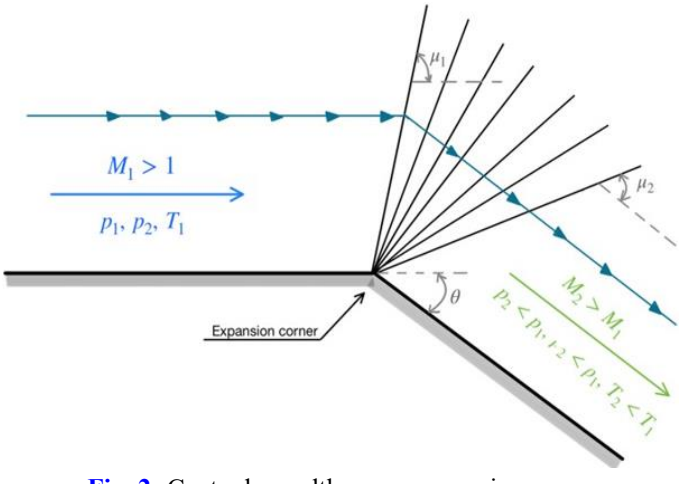

Fig. 2: Centred prandtl-meyer expansion wave.

For the isentropic flow through an expansion wave, M_1 and M_2 are upstream and downstream Mach numbers, respectively. Hence, the Prandtl-Meyer equation depends on M and γ as below:

$$f_1 = \sqrt{\frac{\gamma+1}{\gamma-1}}tan^{-1}\sqrt{\frac{\gamma-1}{\gamma+1}(M^2-1)} - tan^{-1}\sqrt{M^2-1} \quad (17)$$

$$f_2 = f_1 + \theta \quad (18)$$

where f stands for the Prandtl-Meyer function, and θ is the flow deflection angle. The pressure, temperature and density behind the wave can be calculated using isentropic flow equations once M_2 is obtained, as follows:

$$p_2 = p_1\left[\frac{1+\left(\frac{\gamma-1}{2}\right)M_1{}^2}{1+\left(\frac{\gamma-1}{2}\right)M_2{}^2}\right]^{\frac{\gamma}{(\gamma-1)}} \quad (19)$$

$$T_2 = T_1\frac{1+\left(\frac{\gamma-1}{2}\right)M_1{}^2}{1+\left(\frac{\gamma-1}{2}\right)M_2{}^2} \quad (20)$$

By solving equations from (1) to (4), numerically, the aerodynamic heating coefficient and surface temperature distribution on the body surface can be obtained.

When the Mach number of the flow becomes $Ma_\infty \gg 1$, hypersonic speed is experienced, and phenomena such as high-temperature flow, thin shock, and entropy layers, and severe aerodynamic heating occur.

The aerodynamic drag on the blunt body is calculated from the simulations, using the reference parameters values of Mach number, $M = 6$, inlet flow pressure, $M_\infty = 8.3 \times 10^5 pa$, inlet flow temperature, $T_\infty = 450\,K$ and Reynolds number of $Re_L = 0.5 \times 10^6$ based on spike length, $L = 6cm$, at angle of attack of α=0º, 5º and 8º. The other flow parameters, such as density, viscosity, and Prandtl number, have been calculated at $T_\infty = 450\,K$. During the simulations, axial (A) and normal (N) forces are computed and then used to calculate the aerodynamic drag force and drag coefficient as follows:

$$D = N\,Sin\,\alpha + \mathrm{A}\cos\alpha \quad (21)$$

$$C_D = \frac{D}{q_\infty \times S} \quad (22)$$

where D is the aerodynamic drag force, (N), C_D is the aerodynamic drag coefficient, q_∞ is the free stream dynamic pressure and $q_\infty = 0.5\rho V_\infty^2\ (Pa)$, and S is the reference area (m^2).

Furthermore, the pressure distributions on the blunt body are measured as a function of the free stream dynamic pressure as follows,

$$C_\mathrm{P} = \frac{P-P_\infty}{q_\infty} \quad (23)$$

where P is the measured local pressure (Pa) and P_∞ is the free stream pressure (Pa).

2.5 Validation dataset

To validate the CFD model used in the current study, the experimental data provided by Kalimuthu, R., R. C. Mehta, and E. Rathakrishnan is taken as reference results.[22] In the experimental study, three different spike tips; conical aerospike, hemisphere aerodisk and flat-faced aerodisk with L/D ratios equal to 1.5 and 2.0 were tested at various AOA ($\alpha = 0°, 5°$ and 8°). The blunt body had a hemispherical nose, and all experiments were performed at a Mach number of 6. Technical details of the model's geometry and testing operating conditions are given in another study published by the same authors.[10] The experimental results show that the combination of flat-faced aerodisk with L/D ratio equal to 2.0, exhibit the best C_D results for the studied range of AOA, hence it is selected to be used for validation.

2.6 Numerical model setup

The hypersonic flow field around the spiked blunt body was simulated by solving the compressible Navier-Stokes equations in ANSYS Fluent Solver using a fully unstructured finite volume solver. Roe flux-difference splitting (Roe-FDS) Scheme with second-order discretization was used.[23] This scheme is second-order central difference with added matrix dissipation term that produces an up-winding pressure and flux velocity in supersonic and hypersonic flow, hence, better shock capturing compared to the AUSM flux type. Density-

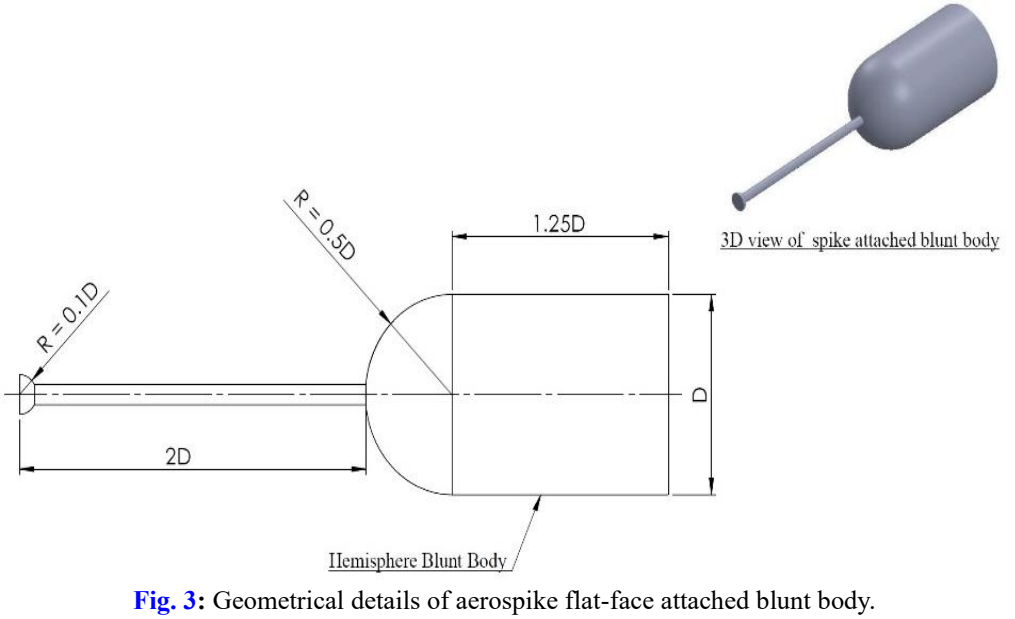

Fig. 3: Geometrical details of aerospike flat-face attached blunt body.

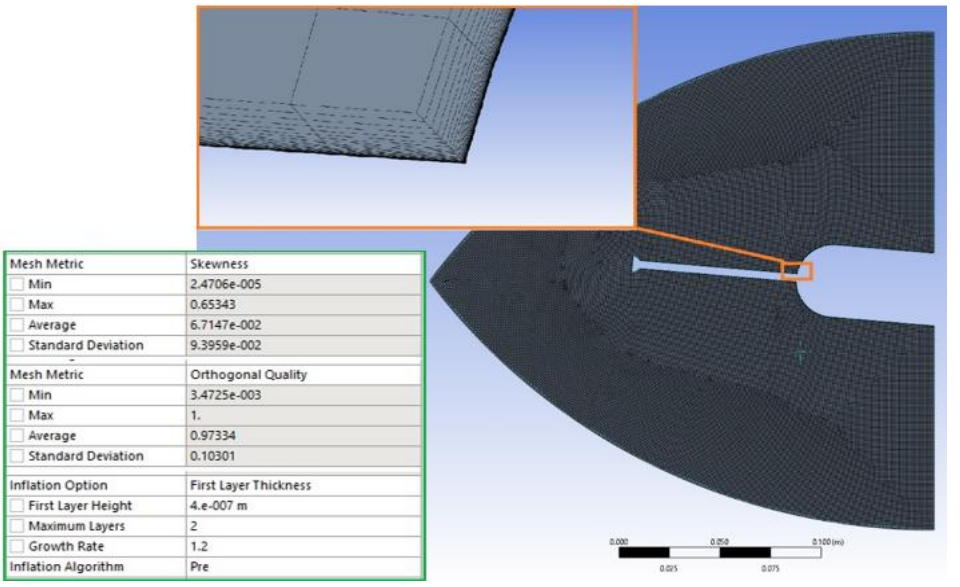

Fig. 4: Computational domain with structure grid, inflation layers and mesh parameters.

based implicit formulation approach with Courant number of 0.9 is selected. The physical geometry fused in the numerical simulations is created in DesignModeler based on the experimental work as shown in Fig. 3. The enclosure is created similar to the hypersonic enclosed free jet wind tunnel, as shown in Fig. 4.

The height of the enclosure set to 254 mm with small with very fine structure mesh to ensure the aspect ratio, skewness, and orthogonal quality are within the suggested range. The skewness value is 0.067 on average, and the orthogonal quality is 0.973. Free stream Mach number of 6, temperature of 450 K and inlet pressure far field of 8.3×10^5 Pa are set at the inlet boundary conditions. The outlet pressure of 1.0 atm and the temperature of 300 K are set at the outlet boundary conditions. The reference values, such as reference length, were based on the length of the blunt body. The reference area is used as the wet area of the blunt body.

2.7 Validation of the drag

Fig. 5 shows a comparison of the drag coefficient results between experimental data and CFD simulation results for a single aerospike. As can be seen, there is a decent agreement between the two results, and the error was calculated as less than 7.4%. Furthermore, the comparison of the experimental Schlieren pictures and the density contours obtained from CFD simulations is shown in Fig. 6. The expected areas, such as bow shock wave, recirculation region and shear layer, can be clearly seen and identified in the CFD results. The recirculation region in the simulation results is slightly bigger than its counterpart from the experiments. Moreover, the generated bow shock wave is broader compared to experimental results. Hereby, the re-attachment shock wave is away from the blunt body compared to experimental results. Furthermore, the shock-shock interaction occurs on the lower frontal area of the blunt body in the experiment at 5° and 8° AOA. However, the shock-shock interaction in the simulation results is located slightly away from the blunt body, and this location is marked as a cross in Fig. 6c for both the

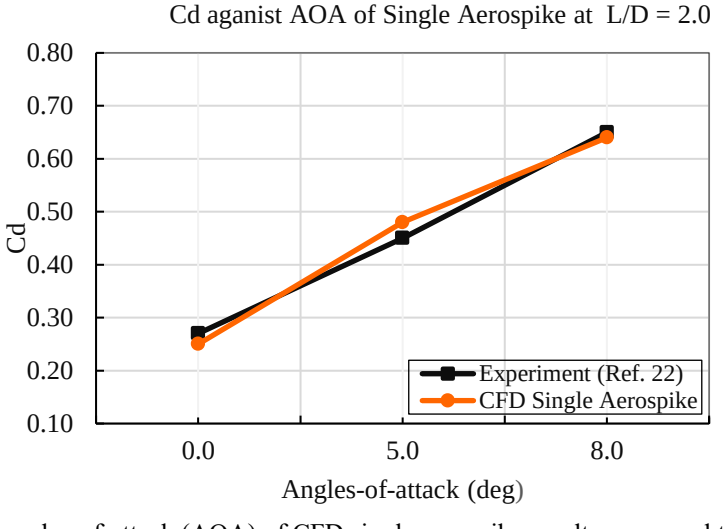

Fig. 5: Cd against angles-of-attack (AOA) of CFD single aerospike results compared to experimental data.[22]

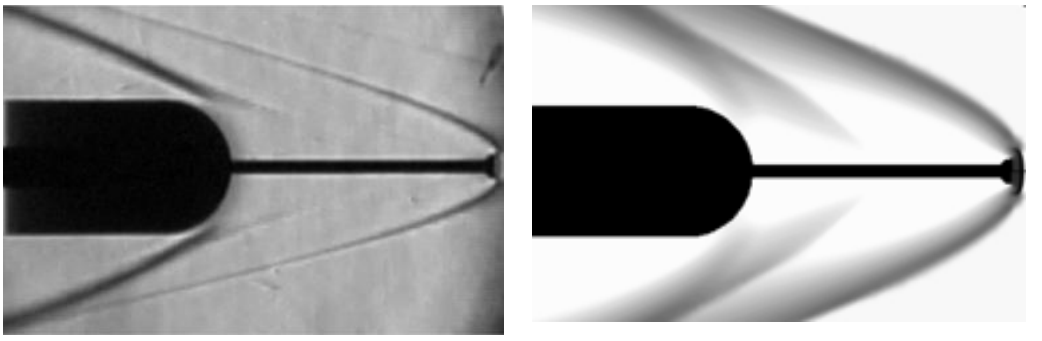

(a) $\alpha = 0°$

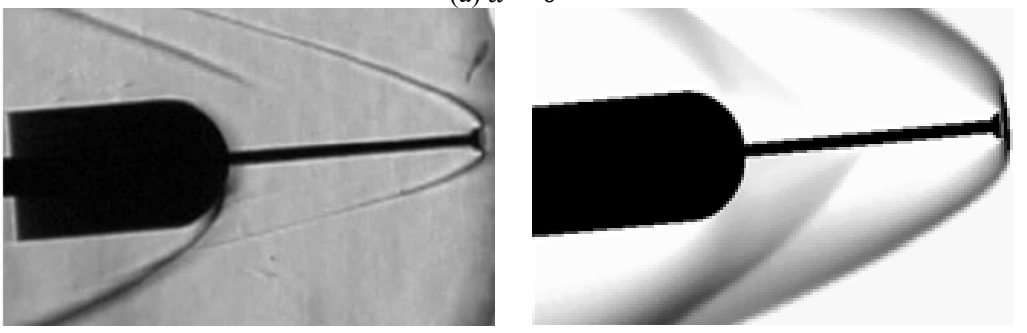

(b) $\alpha = 5°$

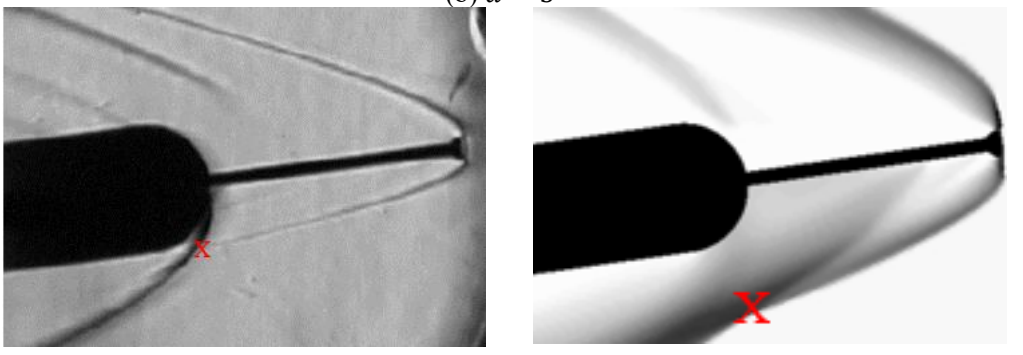

(c) $\alpha = 8°$

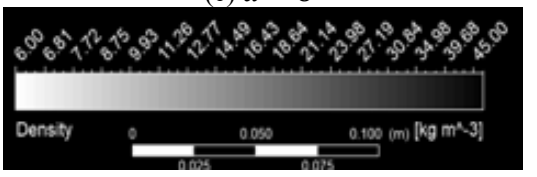

Fig. 6: Schlieren pictures [22] (left) and CFD density contours (right) for flat-faced aerodisk at L/D=2.0.

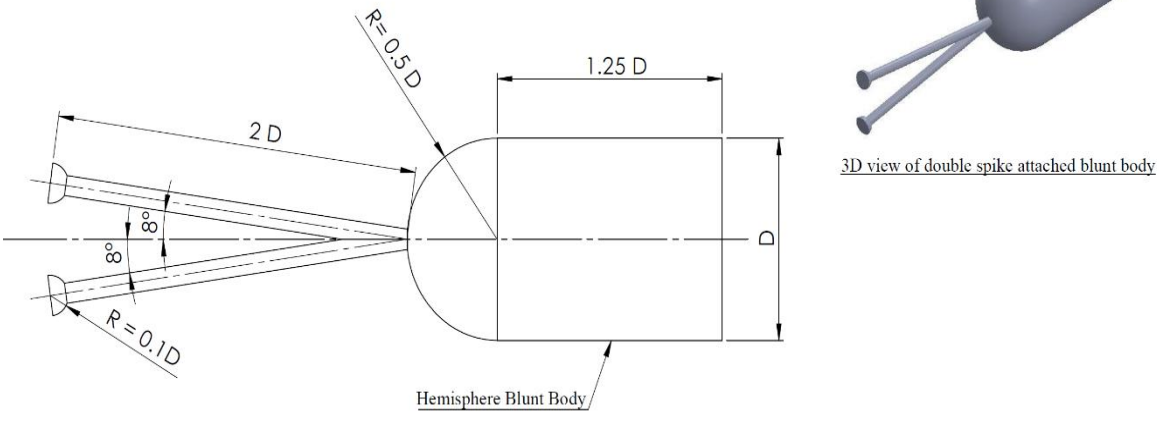

Fig. 7: Geometrical details of double-aerospike flat-face attached blunt body.

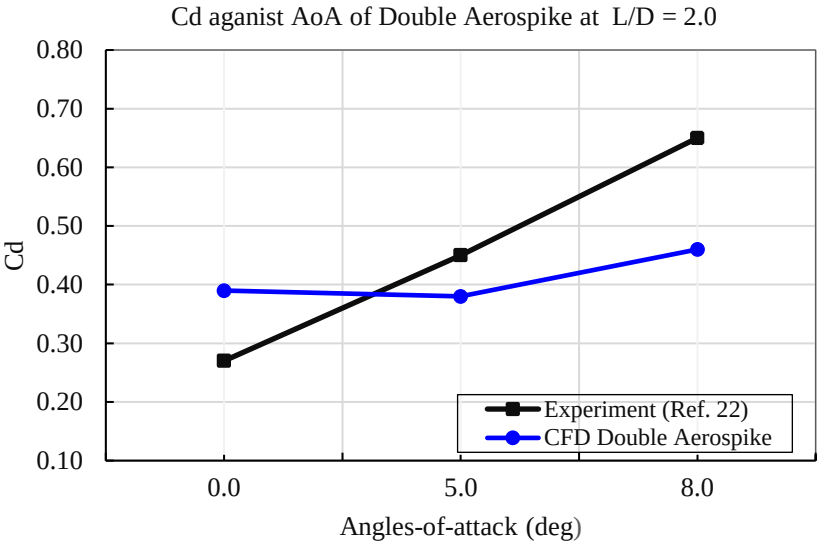

Fig. 8: Cd against AOA of CFD double aerospike results compared to experimental data.[22]

experiments and the simulations.

Based on the C_D results and the comparison between schlieren pictures from the experiments and density contours from CFD simulation for single aerospike, there is clear evidence that the numerical methods and algorithms applied in the current CFD model are accurate and correctly implemented to predict the aerodynamic drag and flowfield for supersonic flow and can be used effectively for investigating the novel double-aerospike method.

3. Results and discussion

3.1 Novel double aerodisk model

In the last two decades, loads of experiments and numerical work have been carried out to study the effect of aerospike on hypersonic drag reduction. The results concluded that even if different tip combinations were used, the aerospike method did not meet the expectations of the researchers. Also, when researchers applied a lateral jet at the aerospike's tip, the results were not as expected.[44,45] Therefore, the current research aims to have a better drag coefficient and aerodynamic heat reduction results by applying a novel double aerospike with a flat-faced tip attaching to the blunt nose of a hypersonic vehicle. Since the literature showed that the aerospike behaved well at 8° AOA,[22,46] hence the novel double aerospike is attached to the blunt body at $\pm 8.0°$ relative to the blunt body's centreline, as shown in Fig. 7. The geometrical details of aerospike, aerospike's tip and the blunt body are kept the same as what has been used in the validation section. Moreover, The flow properties and operating conditions of hypersonic are kept the same as stated in the experimental work.[22] On the other hand, reference values and numerical algorithms are also used as what have been implemented in the validation simulation part. The CFD simulation results obtained from applying the novel double-aerospike method are compared against the experimental data.

3.2 Drag

Fig. 8 shows the drag coefficient results obtained from CFD simulations of the novel double aerospike method at α=0°, 5°, and 8° compared against the experimental data of a single aerospike at the same geometrical and operating conditions. The results show that although the predicted drag coefficient results are increased by 45% at 0° AOA, it significantly reduced by 15.55% and 29.23% at 5° and 8° AOA, respectively. The novel approach of implementing the double aerospike at the hemispherical nose of hypersonic vehicles has shown promising results at an angle of attack greater than zero.

3.3 Flow field visualisation

Figs. 9, 10 and 11 show comparison of predicted contours of Mach number, pressure and density for hypersonic flow over double and single aerospike at L/D=2.0 and different angles of attack, respectively. The comparisons show that the flat-faced attached single aerospike had better C_D results at zero angle of attack, $\alpha = 0°$. However, the novel double aerospike presented promising results and drag reduction performance when angle of attack became more than zero ($\alpha = 5° \& 8°$). It can be argued from the results shown in Fig. 8, that the overall reduction in drag at higher angles of attacks ($\alpha = 5° \& 8°$) for the double aerospike configuration is much substantial than the slightly increased drag at $\alpha = 0°$, hence making the double aerospike configuration a more suitable candidate for better aerodynamic flight characteristics.[22- 47]

The results also display the effect of implementing of the novel double aerospike in front of the blunt body and how the conical shock wave has pushed further away from the blunt body as compared to the cases of using single aerospike at the same angle of attack. The behaviour of bow shock wave can be observed clearly in density contours in Fig. 11. In case of using double aerospike (DS) model, the bow shock wave widely increased and created a "shield shock wave" at the

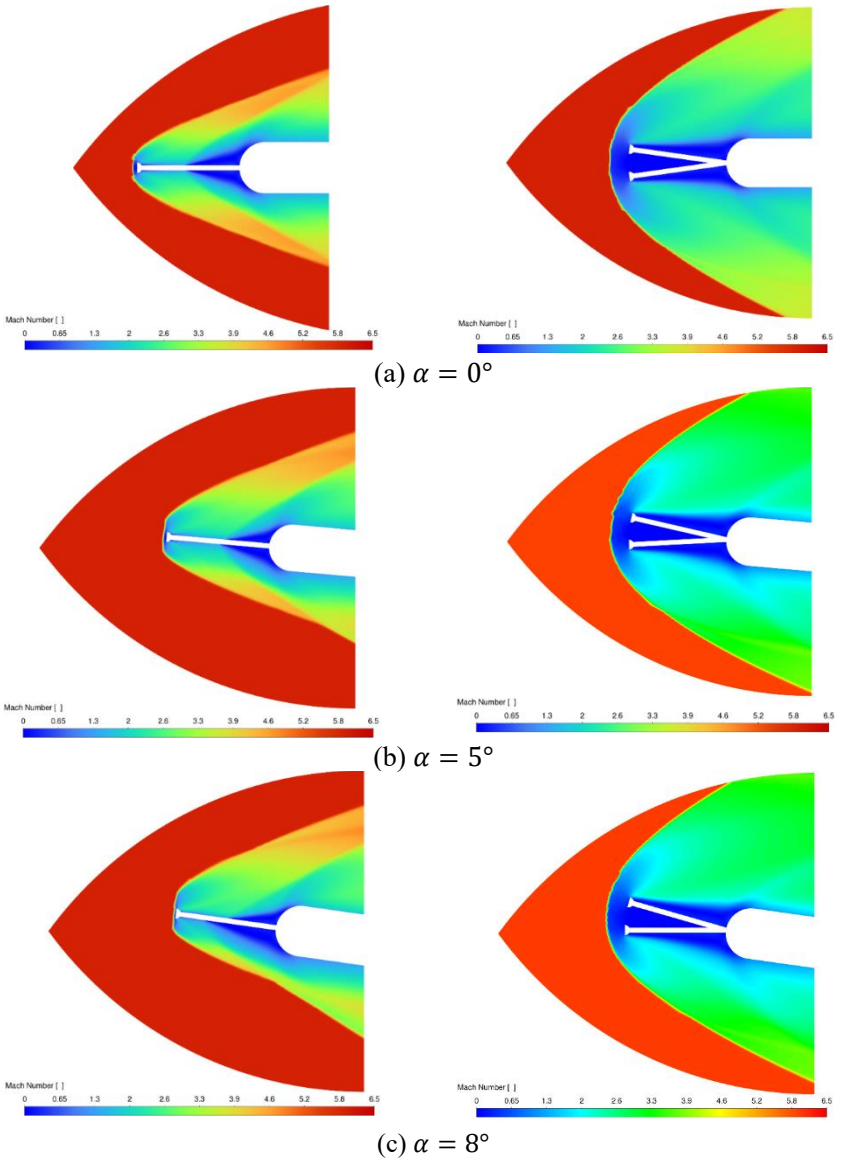

Fig. 9: Comparison of predicted Mach number contours for flat-faced single and double aerospike at L/D=2.0 and different angle of attack.

forefront of the blunt body compared to the single aerospike (SS) model. Moreover, the shock-shock interaction point that can be unambiguously seen in the SS model has almost disappeared in DS model. Consequently, the reattachment shock wave continued to move parallel to the "shield-shock wave". Also, the behaviour of "shield shock wave" in the upper and lower zones of the DS model is far more symmetrical compared to the bow shock wave of the SS model. The figures also reveal that the leading shock wave of the DS model has a shield effect at all studied AOA ($\alpha = 0^{\circ}, 5^{\circ}$ & 8°).

The reattachment shock wave is closer to the hemispherical body in the lower zone than the upper zone at AOA of 8°. However, at AOA of 5°, the behavior of reattachment shock wave at the upper and lower zones is closer to symmetrical conditions. Lastly, the reattachment shock wave at 0° AOA behaves fully balanced. The behaviour of the leading shock wave can be explained from the flowfield behaviour in the region between the two arms of double aerospike model, where the Mach number is almost zero. This means the flow in that region creates vortices and the velocity is almost zero. Hence, the double aerospike arms behave like blocks, and these blocks generate a broader leading shock wave called a "shield shock wave". For all studied angle of attack, the maximum pressure is observed in front of the flat faced tip of the SS model, whereas the maximum pressure has occurred between the two aerospike arms in DS model. The simulation results showed that the maximum pressure of the DS model dropped by 44.15%, 33.55% and 43.28%. at $\alpha = 0^{\circ}, 5^{\circ}, 8^{\circ}$, respectively.

The concentration of heat and pressure near the model tip in case of using double aerospike could increase the ablation of the aerospike and lead to structural failure.[48,49] Non-ablative thermal protection system (NaTPS) have been proposed in the past by researchers as an effective solution for excessive aero heating problem in hypersonic vehicles. These systems consist of a combination of a spike-blunt body and

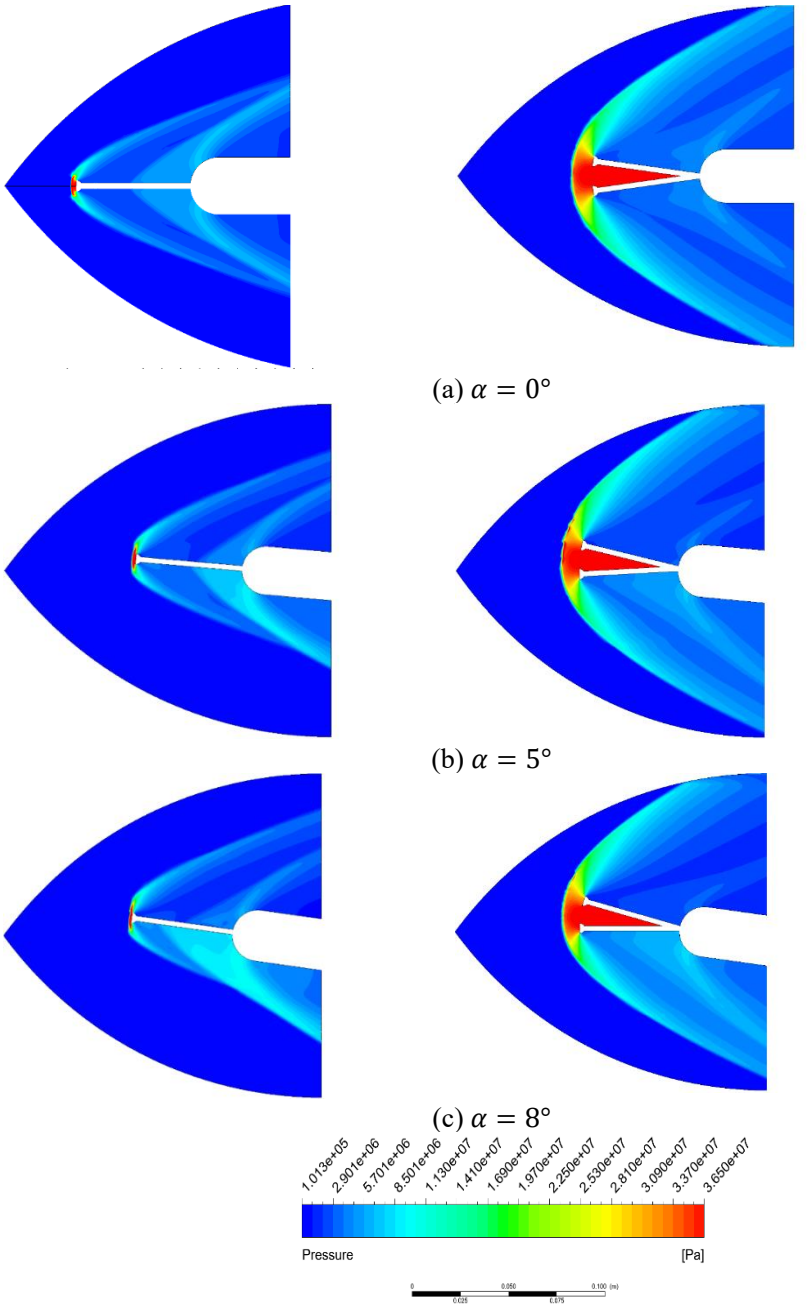

Fig. 10: Comparison of predicted pressure contours for flat-faced single and double aerospike at L/D=2.0 and different angle of attack.

lateral jets to develop a new shock-reconstructing system ahead of the blunt body. The lateral jets are used for pushing the conical shock wave from the hypersonic vehicle surfaces.[44,49]

3.4 Thermal field

Eventually, the heat distribution reduction over the blunt body is one of the main targets of the aerospike attaching concept. The predicted maximum temperature results over the upper and lower frontal areas (FA) of the hemispherical body at $\alpha = 0^{\circ}, 5^{\circ}$ & 8° for single aerospike (SS) and novel double aerospike (DS) models are outlined in Table 2. As it can be seen from the table, the maximum temperature distribution over the upper and lower frontal areas (FA) of the hemispherical body at $\alpha = 0^{\circ}$ is identical, however it differs at $\alpha = 5^{\circ}$ & 8° for SS model. The results also show that the use of DS model reduces the aerodynamic heating around the hemispherical body at all studied angle of attack $\alpha = 0^{\circ}, 5^{\circ}$ & 8° and the difference in maximum temperature distribution over the upper and lower frontal areas (FA) are $0.12\ K, 47.82\ K$ & $7.98\ K$, respectively. This sensible reduction in aerodynamic heating is promising to acknowledge the use of the current novel DS model in hypersonic vehicles. The significant temperature difference between upper and lower frontal areas of blunt body is obtained for SS model at 8° AOA, which was $212.67\ K$. However, the novel DS model reduced that difference with $7.98\ K$ lower than the maximum temperature difference in

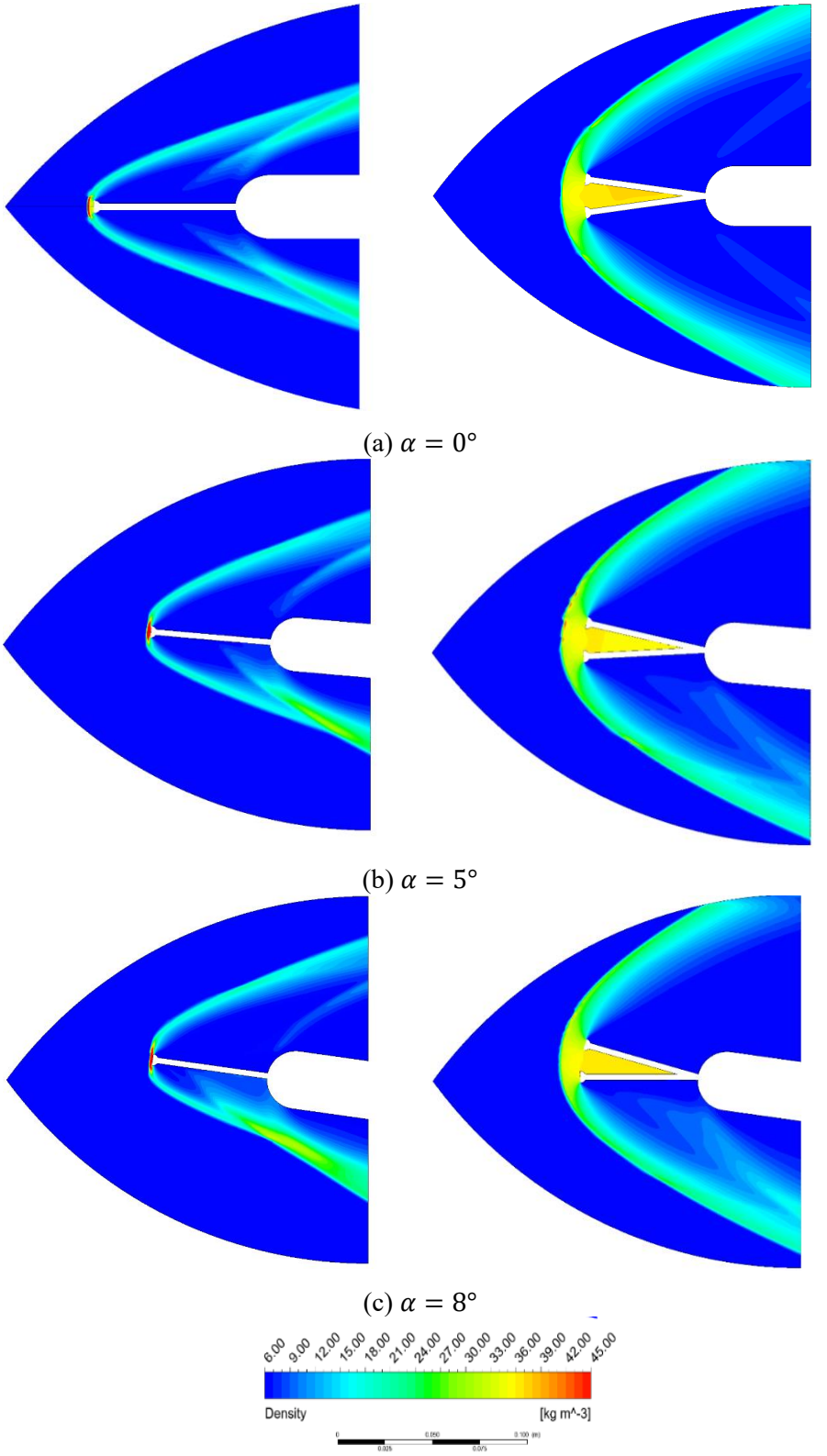

Fig. 11: Comparison of predicted density contours for flat-faced single and double aerospike at L/D=2.0 and different.

Table 2: Maximum temperature over the blunt body models with Single and Double aerospike at various AOA.

	Single Aerospike (SS)			Double Aerospike (DS)		
$\alpha\ (deg)$	Upper Temp (K)	Lower Temp (K)	$\triangle T\ (K)$	Upper Temp (K)	Lower Temp (K)	$\triangle T\ (K)$
0°	3716.41	3716.41	0.0	3563.44	3563.56	0.12
5°	3593.25	3600.20	6.95	3565.49	3613.29	47.82
8°	3705.42	3492.75	212.67	3603.14	3595.16	7.98

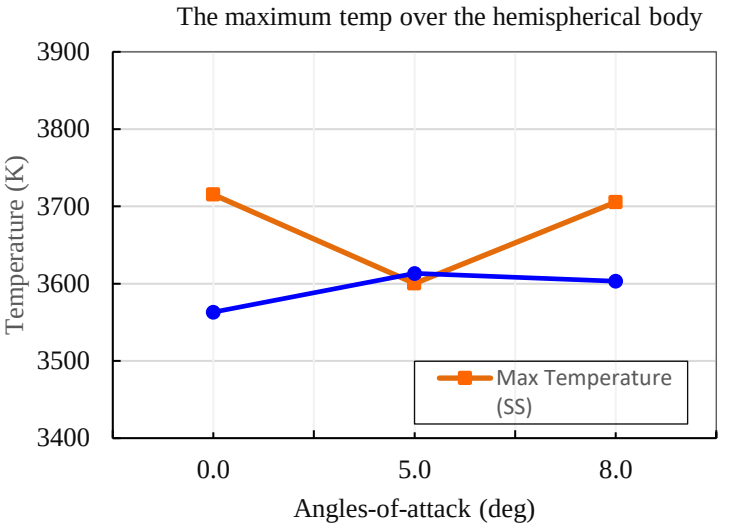

Fig. 12: Comparison of maximum heat over the blunt body with SS and novel DS models attached.

case of the SS model at 8°. That means, the novel DS model reduced the temperature difference by 96.25% at 8° compared to the SS model, which is considered as the most effective heat reduction result in this study.

Comparison of the maximum temperature measured over the hemispherical body in case of attaching SS model and novel DS models is depicted in Fig. 12. The figure shows that the use of novel DS model reduced the maximum heat generated over the blunt body at $\alpha = 0^{\circ}$ & 8° with 4.1% & 2.76% , respectively compared to the use of SS model. However, the maximum heat generated over the blunt body increased by $13.09\,K$ with using the novel DS model compared to the SS model at $\alpha = 5^{\circ}$, as shown from the predicted temperature contours over the blunt body in Fig. 13.

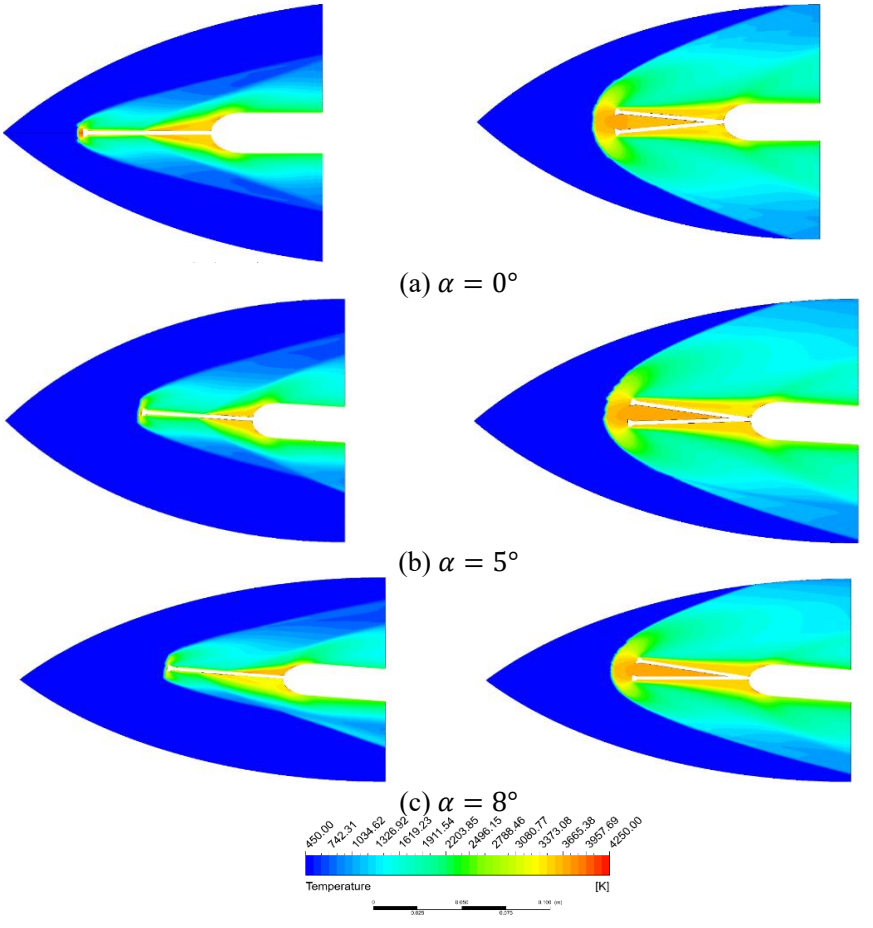

Fig. 13: Predicted temperature contours for flat-face SS and novel DS at L/D=2.0 and different angles of attack.

4. Conclusion

The present study numerically looked at the double aerospike (DS) on the performance of hypersonic vehicles. There was a good agreement between the simulations and the experimental data. In light of the novel DS results, the drag coefficient was significantly reduced compared to the single aerospike (SS) by 15.55% and 29.23% at 5° and 8° AOA, respectively. Moreover, the maximum aerodynamic heat generated was also reduced compared to the SS model by 4.1% and 2.76% at 0° and 8° AOA, respectively. It was observed that with the use of the DS model, the heat distributed over the blunt body's upper and lower frontal areas was more symmetrical than the case of using the SS model. This symmetrical behavior of the heat distribution caused a sensible reduction in the temperature difference ($\triangle T$) and gave more predictable results for the thermal distribution. This promising behavior of the DS model in terms of drag and heat reduction can be attributed to the increase in the width of the bow shock wave which created a "shield shock wave" at the forefront of the blunt body; this shield acts as a barrier protecting the hemispherical body. Consequently, the study of the double spike attached model is considered a novel, promising concept to carry on further investigations using both experiments and computational analysis.

Conflict of Interest

There is no conflict of interest.

Supporting Information

Not applicable.

Nomenclature

C_D	drag coefficient
C_P	pressure coefficient
D	diameter of the blunt body [m]
d	aerodisk diameter, m
E_t	total energy per unit volume [J/m^3]
K	temperature degree [Kelvin]
k	thermal conductivity of the material [W/m.K]
L	length of the spike [m]
L/D	spike length-to-diameter of blunt body
M	Mach number
P	pressure [Pa]
P_T	Prandtl Number
q	local heat flux [W.m^2]
q	dynamic pressure [Pa]
Re_L	Reynolds number based on spike length
S	surface area [m^2]
T	Temperature [K]
u	velocity components along the x-axis [m/s]
V	flow velocity [m/sec]
v	velocity components along the y-axis [m/s]
Latin symbols	
θ	angle measured from the centreline [deg]
α	angle of attack [deg]
μ	flow dynamic viscosity [Pa.s]
ρ	flow density [kg/ m^3]
ν	flow kinematic viscosity [m^2/s]
γ	ratio of specific heats, ($\gamma = C_p/C_v$)
τ	wall shear stress [N/m^2]
σ	normal stress [N/m^2]
$\Gamma\|\hat{A}\|$	Roe- averaged values
Subscripts	
f	friction
∞	freestream conditions
w	wall
x	x-axis in Cartesian coordinate system
xx	normal stress in x-direction on a surface with normal is in the x-direction
yy	normal stress in y-direction on a surface with normal is in the y-direction
xy	shear stress in y-direction on a surface with normal is in the x-direction
yx	shear stress in x-direction on a surface with normal is in the y-direction
y	y-axis in Cartesian coordinate system
t	total, turbulent

References

[1] S. Candel, Concorde and the future of supersonic transport, *Journal of Propulsion and Power*, 2004, **20**, 59-68, doi: 10.2514/1.9180.

[2] A. F. P. Houwing, D. R. Smith, J. S. Fox, P. M. Danehy, N. R. Mudford, Laminar boundary layer separation at a fin-body junction in a hypersonic flow, *Shock Waves*, 2001, **11**, 31-42, doi: 10.1007/PL00004055.

[3] K. Satheesh, G. Jagadeesh, Effect of concentrated energy deposition on the aerodynamic drag of a blunt body in hypersonic flow, *Physics of Fluids*, 2007, **19**, 031701, doi: 10.1063/1.2565663.

[4] B. Shen, W. Liu, L. Yin, Drag and heat reduction efficiency research on opposing jet in supersonic flows, *Aerospace Science and Technology*, 2018, **77**, 696-703, doi: 10.1016/j.ast.2018.03.051.

[5] V. N. Kulkarni, V. I. Menezes, K. P. J. Reddy, Effectiveness of aerospike for drag reduction on a blunt cone in hypersonic flow, *Journal of Spacecraft and Rockets*, 2010, **47**, 542-544, doi: 10.2514/1.48159.

[6] J. J. Sebastian, A. Suryan, H. D. Kim, Numerical analysis of hypersonic flow past blunt bodies with aerospikes, *Journal of Spacecraft and Rockets*, 2016, **53**, 669-677, doi: 10.2514/1.a33414.

[7] M. K. Esfeh, S. M. Tajalli, P. Liu, Evaluation of aerospike for drag reduction on a blunt nose using experimental and numerical modeling, *Acta astronautica*, 2019, **160**, 656-671, doi: 10.1016/j.actaastro.2019.03.010.

[8] D. M. Bushnell, Shock wave drag reduction, *Annual Review Of Fluid Mechanics*, 2004, **36**, 81-96, doi:

10.1146/annurev.fluid.36.050802.122110.
[9] M. Gauer, A. Paull, Numerical investigation of a spiked blunt nose cone at hypersonic speeds, *Journal of Spacecraft and Rockets*, 2008, **45**, 459-471, doi: 10.2514/1.30590.
[10] R. Kalimuthu, R. C. Mehta, E. Rathakrishnan, Drag reduction for spike attached to blunt-nosed body at Mach 6, *Journal of Spacecraft and Rockets*, 2010, **47**, 219-222, doi: 10.2514/1.46023.
[11] S. Alexander, Results of tests to determine the effect of a conical windshield on the drag of a bluff body at supersonic speeds, National Aeronautics and Space Administration Hampton Va Langley Research Center, 1947.
[12] D. Beastall, J. Turner, The effect of a spike protruding in front of a bluff body at supersonic speeds, 1952.
[13] J. J. Jones, Flow separation from rods ahead of blunt noses at Mach number 2.72, 1952.
[14] W. A. Mair, LXVIII. Experiments on separation of boundary layers on probes in front of blunt-nosed bodies in a supersonic air stream, *The London, Edinburgh, and Dublin Philosophical Magazine and Journal of Science*, 1952, **43**, 695-716, doi: 10.1080/14786440708520987.
[15] D. J. Maull, Hypersonic flow over axially symmetric spiked bodies, *Journal of Fluid Mechanics*, 1960, **8**, 584, doi: 10.1017/s0022112060000815.
[16] M. S. Holden, Experimental studies of separated flows at hypersonic speeds. II - Two-dimensional wedge separated flow studies, *AIAA Journal*, 1966, **4**, 790-799, doi: 10.2514/3.3548.
[17] R. A. Guenther, J. P. Reding, Fluctuating pressure environment of a drag reduction spike, *Journal of Spacecraft and Rockets*, 1977, **14**, 705-710, doi: 10.2514/3.57253.
[18] V. N. Myshenkov, Numerical investigation of separated flow in front of a spiked cylinder, *Fluid Dynamics*, 1981, **16**, 938-942, doi: 10.1007/BF01089728.
[19] J. Shoemaker, Aerodynamic spike flowfields computed to select optimum configuration at Mach 2.5 with experimental validation, 28th Aerospace Sciences Meeting, 1990.
[20] M. Yamauchi, K. Fujii, F. Higashino, Numerical investigation of supersonic flows around a spiked blunt body, *Journal of Spacecraft and Rockets*, 1995, **32**, 32-42, doi: 10.2514/3.26571.
[21] R. C. Mehta, Numerical analysis of pressure oscillations over axisymmetric spiked blunt bodies at Mach 6.80, *Shock Waves*, 2002, **11**, 431-440, doi: 10.1007/s001930200127.
[22] R. Kalimuthu, R. C. Mehta, E. Rathakrishnan, Experimental investigation on spiked body in hypersonic flow, *The Aeronautical Journal*, 2008, **112**, 593-598, doi: 10.1017/s0001924000002554.
[23] F. Deng, Z. Jiao, B. Liang, F. Xie, N. Qin, Spike effects on drag reduction for hypersonic lifting body, *Journal of Spacecraft and Rockets*, 2017, **54**, 1185-1195, doi: 10.2514/1.a33865.
[24] F. Deng, F. Xie, N. Qin, W. Huang, L. Wang, H. Chu, Drag reduction investigation for hypersonic lifting-body vehicles with aerospike and long penetration mode counterflowing jet, *Aerospace Science and Technology*, 2018, **76**, 361-373, doi: 10.1016/j.ast.2018.01.039.
[25] D. Sahoo, S. Das, P. Kumar, J. K. Prasad, Effect of spike on steady and unsteady flow over a blunt body at supersonic speed, *Acta Astronautica*, 2016, **128**, 521-533, doi: 10.1016/j.actaastro.2016.08.005.
[26] Z. G. Wang, X. W. Sun, W. Huang, S. B. Li, L. Yan, Experimental investigation on drag and heat flux reduction in supersonic/hypersonic flows: A survey, *Acta Astronautica*, 2016, **129**, 95-110, doi: 10.1016/j.actaastro.2016.09.004.
[27] X. Sun, W. Huang, M. Ou, R. Zhang, S. Li, A survey on numerical simulations of drag and heat reduction mechanism in supersonic/hypersonic flows, *Chinese Journal of Aeronautics*, 2019, **32**, 771-784, doi: 10.1016/j.cja.2018.12.024.
[28] H. Zhao, K. Peng, Z. Wu, W. Zhang, J. Yang, J. Sun, Numerical simulation of supersonic carman curve bodies with aerospike, *International Journal of Aerospace Engineering*, 2021, **2021**, 8821721, doi: 10.1155/2021/8821721.
[29] N. Abed, I. Afgan, A. Cioncolini, H. Iacovides, A. Nasser, Assessment and evaluation of the thermal performance of various working fluids in parabolic trough collectors of solar thermal power plants under non-uniform heat flux distribution conditions, *Energies*, 2020, **13**, 3776, doi: 10.3390/en13153776.
[30] N. Abed, I. Afgan, A. Cioncolini, H. Iacovides, A. Nasser, T. Mekhail, Thermal performance evaluation of various nanofluids with non-uniform heating for paraboliccitrough collectors, *Case Studies in Thermal Engineering*, 2020, **22**, 100769, doi: 10.1016/j.csite.2020.100769.
[31] N. Abed, I. Afgan, H. Iacovides, A. Cioncolini, I. Khurshid, A. Nasser, Thermal-hydraulic analysis of parabolic trough collectors using straight conical strip inserts with nanofluids, *Nanomaterials*, 2021, **11**, 853, doi: 10.3390/nano11040853.
[32] A. E. A. Ali, I. Afgan, D. Laurence, A. Revell, A dual-mesh hybrid RANS-LES simulation of the buoyant flow in a differentially heated square cavity with an improved resolution criterion, *Computers & Fluids*, 2021, **224**, 104949, doi: 10.1016/j.compfluid.2021.104949.
[33] N. Abed, I. Afgan, A. Cioncolini, H. Iacovides, A. Nasser, Effect of various multiple strip inserts and nanofluids on the thermal–hydraulic performances of parabolic trough collectors, *Applied Thermal Engineering*, 2022, **201**, 117798, doi: 10.1016/j.applthermaleng.2021.117798.
[34] J. D. Anderson, J. Wendt, Computational fluid dynamics, 1995.
[35] H. K. Versteeg, An introduction to computational fluid dynamics the finite volume method, 2/E, Pearson Education India, 2007.
[36] Y. A. Çengel, J. M. Cimbala, R. H. Turner, Properties of fluids, Fluid mechanics: fundamentals and applications, 2014.
[37] D. C. Wilcox, Formulation of the k-w turbulence model revisited, *AIAA Journal*, 2008, **46**, 2823-2838, doi: 10.2514/1.36541.

[38] T. B. Gatski, J. P. Bonnet, Compressibility, turbulence, and high speed flow, 2013.
[39] J. H. Ferziger, M. Perić, R. L. Street, Computational methods for fluid dynamics, 2020.
[40] H. Schlichting, K. Gersten, Boundary-layer theory, 2017.
[41] C. J. Riley, F. R. DeJarnette, Engineering aerodynamic heating method for hypersonic flow, *Journal of Spacecraft and Rockets*, 1992, **29**, 327-334, doi: 10.2514/3.26355.
[42] F. R.Yue, J. Yang, G. Q. Jiang, R. Lu, Aerodynamic heating calculation of micro-gravity rocket, *Guti Huojian Jishu/J. Solid Rocket Technol (China)*, 2003, **26**, 1-3.
[43] J. D. Anderson, Hypersonic and high temperature gas dynamics, 1989.
[44] Y. Liu, Z. Jiang, Concept of non-ablative thermal protection system for hypersonic vehicles, *AIAA Journal*, 2013, **51**, 584-590, doi: 10.2514/1.j051875.
[45] D. H. Crawford, Investigation of the flow over a spiked-nose hemisphere-cylinder at a Mach number of 6.8, 1959.
[46] F. Deng, Z. Jiao, B. Liang, F. Xie, N. Qin, Spike effects on drag reduction for hypersonic lifting body, *Journal of Spacecraft and Rockets*, 2017, **54**, 1185-1195, doi: 10.2514/1.A33865.
[47] M. B. Gerdroodbary, S. M. Hosseinalipour, Numerical simulation of hypersonic flow over highly blunted cones with spike, *Acta Astronautica*, 2010, **67**, 180-193, doi: 10.1016/j.actaastro.2010.01.026.
[48] A. L. Murray, G. W. Russell, Coupled aeroheating/ablation analysis for missile configurations, *Journal of Spacecraft and Rockets*, 2002, **39**, 501-508, doi: 10.2514/2.3862.
[49] Y. Yuan, Z. Cao, B. Fu, Z. Xiao, C. Nie, X. Chen, R. Li, Experimental study on the flow field and aeroheating characteristics induced by a combinational aerospike and multi-jet scheme in large angle of attack, *International Journal of Heat and Mass Transfer*, 2022, **195**, 123131, doi: 10.1016/j.ijheatmasstransfer.2022.123131.

Publisher's Note: Engineered Science Publisher remains neutral with regard to jurisdictional claims in published maps and institutional affiliations.

Open Access

This article is licensed under a Creative Commons Attribution 4.0 International License, which permits the use, sharing, adaptation, distribution and reproduction in any medium or format, as long as appropriate credit to the original author(s) and the source is given by providing a link to the Creative Commons licence and changes need to be indicated if there are any. The images or other third-party material in this article are included in the article's Creative Commons licence, unless indicated otherwise in a credit line to the material. If material is not included in the article's Creative Commons licence and your intended use is not permitted by statutory regulation or exceeds the permitted use, you will need to obtain permission directly from the copyright holder. To view a copy of this licence, visit http://creativecommons.org/ licenses/by/4.0/.

©The Author(s) 2025